FORUM GE GRAFI
Indonesian Journal of Spatial and Regional Analysis

The Relationship between the Mixed Pixel Spectral Value of Landsat 8 OLI Data and LAPAN Surveillance Aircraft (LSA) Aerial-Photo Data

Nurwita Mustika Sari*, Galdita Aruba Chulafak, Zylshal, Dony Kushardono

Remote Sensing Applications Center, Indonesian National Institute of Aeronautics and Space
* Corresponding author (e-mail: nurwita.mustika@lapan.go.id)

Abstract. Medium-resolution satellite data such as data from Landsat has a lot of potential for a mixed pixel (mixel) to occur. Indonesian land use is diverse, especially in urban areas, which causes a high potential for mixels in the Landsat pixel size of 30 x 30m, based on the actual conditions. Multispectral aerial photo data from LAPAN Surveillance Aircraft (LSA) with a spatial resolution reaching 58cm can display objects in more detail in these sizes. The purpose of this research is to study mixels in Landsat 8 Operational Land Imager (OLI) data, with multispectral data from an LSA as a complement to the Landsat 8 OLI data. The method proposed in this study is a visual interpretation using the object-based image analysis (OBIA) method for the classification of land cover, testing the validity of the sample to be used in the research, and then using the normalized difference vegetation index (NDVI) to see the relationship between the vegetation index of the LSA data and the Landsat 8 OLI data. The results showed that the regression equation obtained from the regression between the NDVI of the Landsat 8 OLI data and the NDVI of the LSA with a significance of less than 0.05 is y = 0.732x - 0102 with a value of R^2 = 0.887. Through these results we can conclude that the NDVI values for both sets of data are related to one another.

Keywords: mixed pixel, aerial remote sensing, LSA, Landsat, OBIA, NDVI.

Abstrak. Data satelit beresolusi sedang seperti data dari Landsat memiliki banyak potensi untuk terjadinya piksel campuran (mixel). Penggunaan lahan di Indonesia beragam, terutama di daerah perkotaan, yang menyebabkan potensi mixel tinggi pada ukuran piksel Landsat 30 x 30m, berdasarkan kondisi sebenarnya. Data foto udara multispektral dari LAPAN Surveillance Aircraft (LSA) dengan resolusi spasial mencapai 58cm dapat menampilkan objek secara lebih rinci dalam ukuran ini. Tujuan dari penelitian ini adalah untuk mempelajari mixel dalam data Landsat 8 Operational Land Imager (OLI), dengan data multispektral dari LSA sebagai pelengkap data OLI Landsat 8. Metode yang diusulkan dalam penelitian ini adalah interpretasi visual dengan menggunakan metode analisis citra berbasis objek (OBIA) untuk klasifikasi tutupan lahan, menguji validitas sampel yang akan digunakan dalam penelitian, dan kemudian menggunakan normalized difference vegetation index (NDVI) untuk melihat hubungan antara indeks vegetasi dari data LSA dengan data Landsat 8 OLI. Hasilnya menunjukkan bahwa persamaan regresi yang diperoleh dari regresi antara NDVI data OLI Landsat 8 dan NDVI untuk LSA dengan signifikansi kurang dari 0,05 adalah y = 0,732x - 0102 dengan nilai R^2 = 0,887. Melalui hasil ini, kita dapat menyimpulkan bahwa nilai NDVI untuk kedua kumpulan data saling terkait satu sama lain.

Kata Kunci: piksel campuran, penginderaan jauh udara, LSA, Landsat, OBIA, NDVI.

1. Introduction

The LAPAN Surveillance Aircraft or LSA is an ultra-light aircraft developed by LAPAN, which provides remote sensing as one of its functions. It is capable of acquiring high-resolution imagery in which the objects can be seen very clearly. It helps to produce detailed-scale spatial information, which is

currently required to meet the needs of many sectors, such as infrastructure development for both rural and urban developments, disaster mitigation and agricultural monitoring (Kushardono *et al.*, 2014). Along with these increasing needs, an aerial vehicle that has flexibility in terms of time, flying height and location when performing data acquisition is indispensable. With such a capability, it has much potential to be explored, such as becoming the complement of or comparison to remote sensing satellite data with lower spatial resolution (for example, Landsat) because the objects presented in LSA data may not be visible on Landsat data.

Landsat imagery data is popular data and has been widely used for various kinds of applications, including in research by Sholihah *et al.* (2016), which finds that drought monitoring of agricultural land can be conducted by observing the vegetation health index (VHI). Landsat 8 Operational Land Imager (OLI) has been assessed by the users for looking at the area of hydrothermal alteration in a copper mine. It uses the existing thermal infrared (TIR) band and this data was able to be used to do lithological mapping (Pour and Hashim, 2015). The integrated use of Landsat and LIDAR to map forest structure and biomass was done by Zald *et al.* (2016) in the area of Saskatchewan, Canada, which gained a moderate to high level of accuracy in the model (the value of $R^2 = 0.42$ to 0.69). The use of remote sensing data with different resolutions, namely Landsat and Ikonos, has also been applied to determine soil erosion (Wang *et al.*, 2011). Landsat data has been used for surface-water monitoring in Australia by Mueller *et al.* (2016) following the extreme floods in 2011, which used two decades worth of data and developed standard algorithms based on medium-resolution satellite data for surface water. Landsat data has also been used to evaluate changes in land use/ land cover, which is correlated with the pattern formed by the surface temperature (Lv and Zhou, 2011). Landsat ortho has also been used to validate the model for mapping the wetland area of Lampung province, and the level of accuracy reached 90.6% (Parsa *et al.*,

2014).

The greatest diversity of land cover occurs in urban areas, where the cities are areas with the high physical development of the region as a result of an increasing population (Widodo *et al.*, 2015). The dynamics of the rapid physical development of the city (Mikovits *et al.*, 2014) affects traffic, and one of the affected aspects is the urban road network density (Xing *et al.*, 2013), which also adds to the diversity of land cover in the city. Good urban planning for land use affects the quality of the city, and contains both the complexity of land use and the human activity on it to create a sustainable urban development (Vorontsova *et al.*, 2016).

Such diversity of urban land cover affect to the high possibility of mixture pixel in low resolution imagery. The city as a region of land cover is very diverse; as an example, Bandung, on Green Open Space, just has diversity of land cover, such as areas of trees, mixed garden, farms, bushes/shrubs, open land and paddy fields (Narulita *et al.*, 2016). For this, a study of mixed pixel (mixel) will be needed for further analysis. At Kuningan Regency, West Java, the land cover changes causing narrow boundaries of land cover for the growth of residential areas that are initially homogeneous, consisting of mixed garden or natural forests (Nasihin *et al.*, 2016). Indonesia is a country with a high prospective housing construction market with the regulation and affordability (Monkkonen, 2013).

On the other hand, another area of Indonesia with high diversity of land use/ land cover is the tourist area, including the Gili Matra Island in Lombok, West Nusa Tenggara; this incorporates land use/ land cover such as shoal beaches, sand beaches, salty lakes, mangrove areas, mixed forest, plantations, bare areas, non-built-up areas, settlement areas and tourist accommodation areas. Land conversion into the built-up areas here occurred very fast because of the major influence of the ease of access (Kurniawan *et al.*, 2016).

Landsat data with a resolution of 30m, which includes an area with a high diversity of land cover, has potential for mixels, which actually consist of several objects. The number

of mixels will be higher for imagery data with a coarse resolution (Danoedoro, 2009). The ability of higher-resolution imagery data to display objects in an image well makes the number of pure pixels greater than for low resolution imagery, which tends to have a lot of mixels (Hoyano and Komatsu, 1988).

Mixture can occur in a pixel in various forms, including a boundary between two or more areas of the mapping unit, parts of pixels in the form of a line, parts of pixels in the form of an object and intergrade or changing from one object to another object gradually (Fisher, 1997). Small training data sets containing mixels were used in research using the support vector machine (SVM) method of classification by Foody and Mathur (2006) and obtained an overall accuracy of 92%, which did not differ significantly with the conventional method; therefore, it could be a good alternative, especially in instances where there is difficulty in collecting training data, but is not a replacement for the conventional method. Referring to the research by Hoyano and Komatsu (1988) that divides pixels in several types, including pure pixels, and mixel A and B. Mixel A is composed of several categories and does not have a separate section, while mixel B is a mixel containing several classes/categories and has a separate section.

The use of very-high-resolution remotely sensed data, such as Worldview-2, for the detection of changes in land use (for example, grazing) with Landsat-8 OLI being used as the pre-data will obtain higher accuracy because more specific changes will be detected. It is because the diverse objects will be detected in Worldview-2, while those objects will only be displayed as the same pixel in Landsat-8 OLI (Tarantino et al. 2016). In other research using an object-based method, the separation of objects has been conducted via three methods: the first is based on Landsat 5 Thematic Mapper (TM) and *Satellite Pour l'Observation de la Terre* (SPOT) 5 data, the second is only based on SPOT 5 data and the last is only base on Landsat 5 TM data. Of the three methods, the optimum segment result obtained is based on Landsat 5TM and SPOT 5 and only from SPOT 5.By looking at the

optimum results, it is concluded that using the SPOT 5 data with higher spatial resolution can improve the accuracy from 72.35% to 82.94%. With the increasing accuracy of the result, it is known that high-spatial-resolution data can be used to be a complement of Landsat data (Sun *et al.*, 2014). Study of mixel is important for measuring the accuracy of satellite imagery.

The band on the Tetracam multispectral camera used by the LSA is able to detect vegetation well (Tetracam Inc., 2011). Aerial remote sensing, using an aerial vehicle called an LSA that carried a payload in the form of a Tetracam camera with a spatial resolution of 58cm, has been employed further to see the quality of single-object vegetation in urban areas using the object-based image analysis (OBIA) method and a vegetation index (Sari and Kushardono, 2016), and reached an accuracy of 88%. Besides being used to detect vegetation, LSA multispectral data is capable of displaying objects clearly in the coastal regions (Arifin *et al.*, 2015). LSA multispectral data with a high resolution is a complement to Landsat data, which has a lower resolution to show the estimation of mixel occurring in the Landsat data.

A previous study of mixel, as mentioned before, has already explained the forms of mixel, such as parts of pixels as a line, an object, or an intergrade (which is changing from one object to another object gradually), and another study divides pixel into several types, namely pure pixels, mixel A (which does not have a separate section) and mixel B (which does have a separate section) (Fisher, 1997; Hoyano and Komatsu, 1988), but this study has not completed a stage to determine the relationship of the spectral value between lower-spatial-resolution data and higher-spatial-resolution data. The purpose of this study is to observe the relationship between the mixel spectral value of Landsat 8 OLI data and LSA aerial-photo data.

2. Research Methods
a. Materials

The data used in this study is multispectral image data acquired by the Aeronautic Technology Center's LSA on 19 September 2014

(Figure 1a), which includes the urban areas of Indramayu, West Java and its surroundings, with a spatial resolution of up to 58cm (Table 1).The image data that has been acquired has been processed into mosaics and ortho corrected by the Remote Sensing Application Centre (Kushardono *et al.*, 2014). The other data used is Landsat 8 OLI data acquired on 22 September 2014 (Figure 1b) for the same area. The Landsat data selected is for the closest period to the acquisition of the LSA data and has low cloud cover.
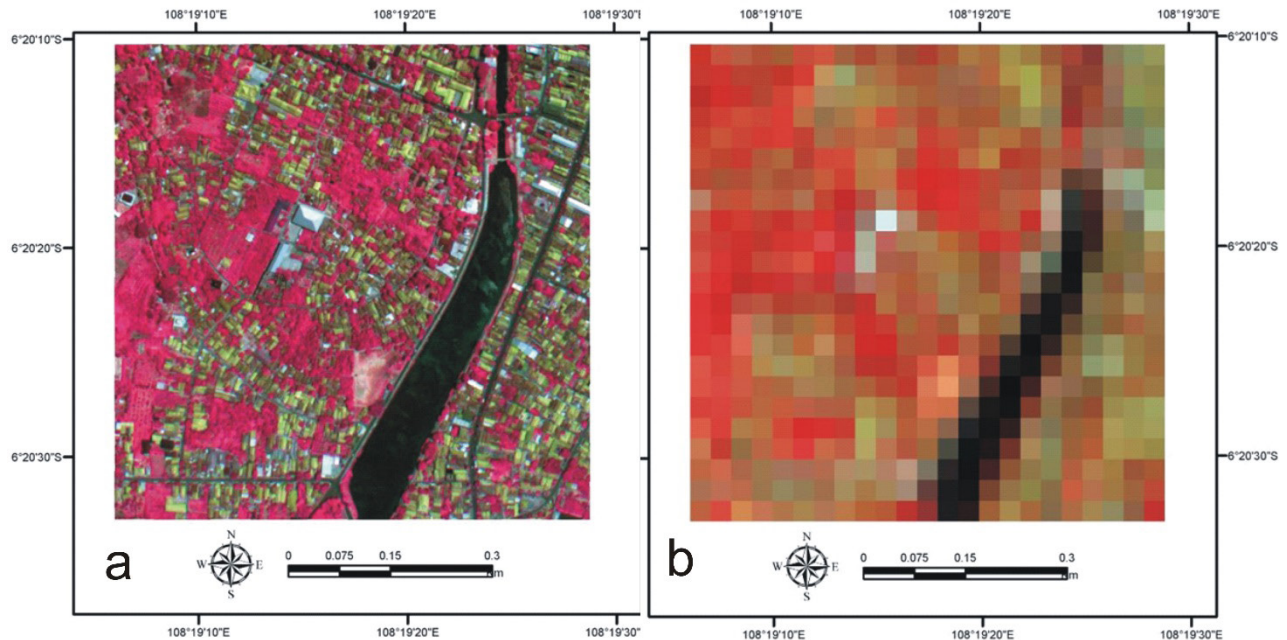
Figure 1. LSA data with colour composite for near infrared (NIR), red, green (a) and Landsat 8 OLI data with colour composite 543 (b)

Table 1. Comparisons of band designations for Landsat 8 OLI and Tetracam multispectral camera used by the LSA

Imagery	Bands	Wavelength (micrometres)	Resolution (metres)
Landsat 8 Operational Land Imager (OLI) and Thermal Infrared Sensor (TIRS)	Band 1 – Ultra Blue (coastal/aerosol)	0.43 – 0.45	30
	Band 2 – Blue	0.45 – 0.51	30
	Band 3 – Green	0.53 – 0.59	30
	Band 4 – Red	0.64 – 0.67	30
	Band 5 – Near Infrared (NIR)	0.85 – 0.88	30
	Band 6 – Shortwave Infrared (SWIR) 1	1.57 – 1.65	30
	Band 7 – Shortwave Infrared (SWIR) 2	2.11 – 2.29	30
	Band 8 – Panchromatic	0.50 – 0.68	15
	Band 9 – Cirrus	1.36 – 1.38	30
	Band 10 – Thermal Infrared (TIRS) 1	10.60 – 11.19	100 * (30)
	Band 11 – Thermal Infrared (TIRS) 2	11.50 – 12.51	100 * (30)

Imagery	Bands	Wavelength (micrometres)	Resolution (metres)
Tetracam Agricultural Digital Camera (ADC) (approx. equal to Thematic Mapper 2,3,4)	Green	0.52-0.60	0.58
	Red	0.63-0.69	
	Near Infrared (NIR)	0.76-0.90	

Source:Tetracam Inc.with modification, US Geological Survey with modification

* TIRS bands are acquired at 100 m resolution, but are resampled to 30 m in delivered data product.

b. Digital Image Processing and Analysis

This research mainly used Landsat 8 OLI data and LSA aerial-photo data for the digital analysis. Figure 2 is the flowchart of the relationship between the mixel spectral values of Landsat 8 OLI data and LSA aerial-photo data, which is further explained in the description of each research stage, such as land cover extraction, atmospheric correction, construct fishnet, sampling, validity assessment of the sample, transformation to NDVI and regression analysis between the NDVI of Landsat and the NDVI of LSA.
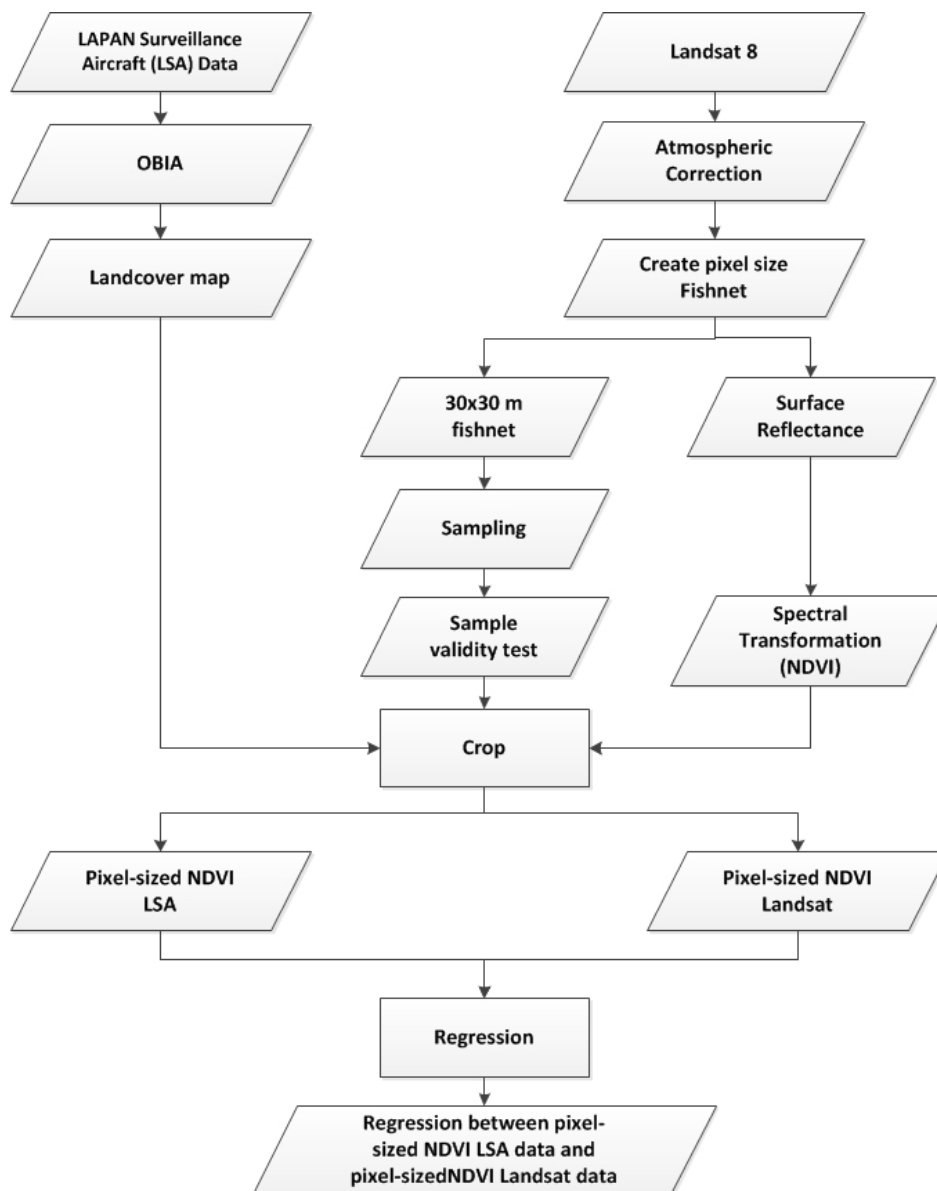

Figure 2. Flowchart of the relationship between the mixel spectral values of Landsat 8 OLI data and LSA aerial-photo data

c. Land Cover Extraction

The extraction of objects used an OBIA method consisting of a segmentation and classification process. The segmentation was done using a multiresolution segmentation algorithm. The multiresolution segmentation has already been used on aerial-photo data and has provided a good result (Sari and Kushardono, 2015). After conducting the segmentation stage, classification was performed using several nearest-neighbour feature spaces (Trimble Doc., 2014):

Mean of layer values

$$\bar{c}_k(v) := \bar{c}_k(P_v) = \frac{1}{\#P_v} \sum_{(x,y)\in P_v} c_k(x,y) \quad (1)$$

where:
Pv is set of pixels of an image object v,
Pv ={(x,y) :(x,y) v},
#Pv is total number of pixels contained in Pv,
 (x,y) is image layer value at pixel (x,y),
$C_k$min is the darkest possible intensity value of layer k,
$C_k$max is the brightest possible intensity value of layer k,
$\bar{c}_k$k is the mean intensity of layer k.

Standard deviation of layer values

$$\sigma_k(v) := \sigma_k(P_v) = \sqrt{\frac{1}{\#P_v}\left(\sum_{(x,y)\in P} c_k^2(x,y) - \frac{1}{\#P_v}\sum_{(x,y)\in P_v} c_k(x,y) \sum_{(x,y)\in P_v} c_k(x,y)\right)} \quad (4)$$

where:
$\sigma_k(v)$ is standard deviation of layer k of an image object v,
P_v is set of pixels of an image object v,
$\#P_v$ is total number of pixels contained in P_v,
$c_k(x,y)$ is image layer value at pixel (x,y),
(x,y) is pixel coordinates,
c_k range is data range of layer k,
c_k range = $c_k$max – $c_k$min.

Mean of brightness

$$\bar{c}(v) := \frac{1}{w^B} \sum_{k-1}^{K} w\binom{B}{k} \bar{c}_k(v) \quad (2)$$

where:
$w\binom{B}{k}$ is the brightness weight of layer k,
$\bar{c}_k(v)$ is the mean intensity of layer k of an image object v,
$c_k$min is the darkest possible intensity value of layer k,
$c_k$max is the brightest possible intensity value of layer k.

Max Diff

$$\frac{\max_{i,j \in K_B} |\bar{c}_i(v) - \bar{c}_j(v)|}{\bar{c}(v)} \quad (3)$$

where:
i, j is image layers,
– $\bar{c}(v)$ is brightness,
– $\bar{c}i(v)$ is mean intensity of layer i
– $\bar{c}_j(v)$ is mean intensity of layer j,
$c_k$max is brightest possible intensity value of layer k,
K_B is layers with positive brightness weight,
K_B ={k □ K : wk=1},
wk is layer weight.

Density

$$d = \frac{\sqrt{\#P_v}}{1 + \sqrt{VarX + VarY}} \quad (5)$$

where:
$\sqrt{\#P_v}$ is diameter of a square object with $\#P_v$ pixels,
$\sqrt{VarX+VarY}$ is diameter of the ellipse.

Compactness

$$C = \frac{l_v * w_v}{\#P_v} \qquad (6)$$

where:
lv is length of an image object v,
wv is width of an image object v, #Pv is total number of pixels contained in Pv.

d.   Atmospheric correction

The atmospheric correction was conducted using the Top of Atmosphere (ToA) correction method, which includes the ToA reflectance and sun angle correction (Rahayu and Candra, 2014). The ToA reflectance correction phase converts the digital number (DN) into a reflectance value.

$$\rho_\lambda' = M_\rho * Q_{cal} + A_\rho \qquad (7)$$

where:
ρ_λ' is ToA planetary reflectance (unitless), without sun angle correction,
M_ρ is reflectance multiplicative scaling factor for the band (REFLECTANCEW_MULT_BAND_N from the metadata),
A_ρ is reflectance additive scaling factor for the band (REFLECTANCE_ADD_BAND_N from the metadata),
Q_{cal} is L1 pixel value in DN.

Then the image is corrected for the sun angle to eliminate the difference in DN values caused by the position of the sun.

$$\rho_\lambda = \frac{\rho_\lambda'}{\cos(\theta SZ)} = \frac{\rho_\lambda'}{\sin(\theta SE)} \qquad (8)$$

where:
ρ_λ is ToA planetary reflectance (unitless),
θSE is solar elevation angle ,
θSZ is solar zenith angle.

e.   Construct a fishnet

Fishnet construction was completed on Landsat data with a pixel size of 30 × 30m. With this fishnet, the process to create a sample and the analysis will be easier and more precise at the same place.

f.   Sampling

The sample selection was conducted using the purposive sampling method that employs specific criteria. A similar sampling method was completed by specifying the criteria for the samples to be taken with a specific purpose. In several studies conducted by Smith *et al*. (2013) and Topp *et al*. (2004), the sample criteria are very specific for sampling the respondents. Furthermore, in the study by Iryadi and Sadewo (2015), land surface area samples are chosen based on certain criteria, including vegetation cover, normalized difference vegetation index (NDVI) class and geomorphology unit. In this case, the total number of samples taken was 35. The selected samples in this study were determined based on vegetation cover within a certain percentage ranging from 0%, which means a pure pixel of non-vegetation land cover, up to 100%, which means it is a pure pixel of vegetation. The number of samples taken was 35 due to those samples being able to represent diverse vegetation cover percentages in the research area. A representative sample of the entire area has a percentage of vegetation cover that varies from 0% to 100%.

g.   Validity assessment of the sample

A sample validity assessment was conducted for the 35 samples selected to undergo a normality test. The validity assessment was conducted using the vegetation area as the primary variable; this validity test was to find out the distribution of samples based on the percentage of vegetation cover. A normality test was conducted using the Shapiro-Wilk test because the sample size was less than 50 (Shapiro and Wilk, 1965).

h.   Transformation to NDVI

NDVI is one of the most commonly used vegetation indexes, with values that are between -1 and 1. The Landsat 8 OLI data and LSA data transformation process to the NDVI value is conducted using a formula that uses

the NDVI value NIR band and the red band value in its calculations (Mokarram *et al.*, 2016). Theoretically, if the NDVI approaches a value of 1, the existing vegetation in that area is greener and denser; if it approaches a value of 0, it means that the vegetation is dry or not green; and if the NDVI value is between 0 and -1, then it is land cover that is not a type of vegetation (Haque and Basak, 2017). The index can be used to detect changes in land cover (Haque and Basak, 2017).

$$NDVI = \frac{NIR - RED}{NIR + RED} \qquad (9)$$

i. Regression analysis between the NDVI of Landisat and the NDVI of LSA

Regression analysis is a statistical process for estimating the relationships among variables, focusing on the functional relationship between a dependent variable and one or more independent variables (Rawlings *et al.*, 2001). Regression analysis was conducted to determine the relationship between the vegetation index of the Landsat 8 OLI data and the vegetation index of LSA data. The NDVI of the LSA data was calculated from the average pixel value from each 30 x 30m fishnet grid to match the Landsat 8 OLI spatial resolution.

3. Results and Discussion

A segmentation process was conducted using a multiresolution segmentation algorithm like in the previous research (Sari and Kushardono, 2015). Object extraction is performed on the LSA data after the object is segmented into 797 objects. The classification process divides the objects into three classes,

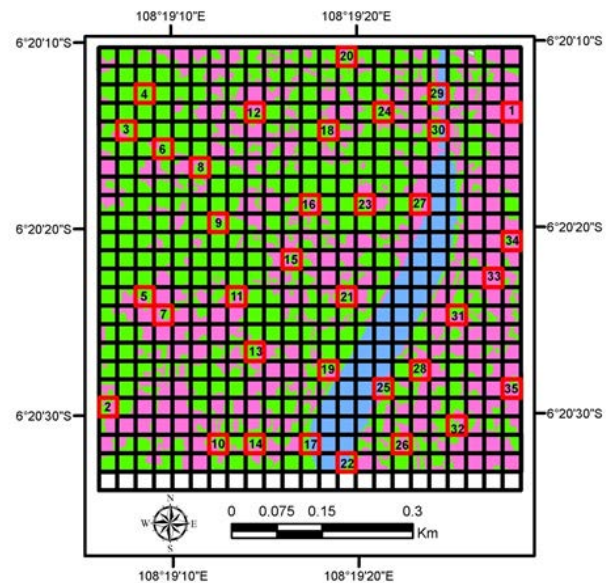water, built up area and vegetation, as shown in Figure 3.

Figure 3. OBIA on the LSA data and sample distribution

The body of water is coloured blue, the built-up area is coloured magenta and the vegetation is coloured. From Figure 3 we can see that the classification result shows the distribution of three land cover classes based on LSA data and there are several class boundaries in one pixel size 30 x 30m. In those adjacent areas, the potential occurrence of mixel is very high.

Based on Table 2, it can be observed that the combinations constructed from Landsat mixels include vegetation and built-up area, body of water and vegetation, body of water and built-up area, and body of water, built-up area and vegetation. In addition, the types of pure pixels consist of vegetation, body of water and built-up area.

Table 2. Classification scheme of the combination

No	Combination
1	Pure pixel of vegetation
2	Pure pixel of a body of water
3	Pure pixel of a built-up area
4	Vegetation & built-up area
5	Body of water & vegetation
6	Body of water & built-up area
7	Body of water & built-up area & vegetation

To conduct further analysis, including sample selection and analysis, a fishnet was constructed with a Landsat pixel size of 30 x 30m. Figure 3 shows the fishnet overlaid onto the classification result. The function of a fishnet/ grid is to make the analysis easier; this was done in previous research, such as in a study in Haiti for the population census area and for modelling in Lake Icaria (Deichmann *et al.*, 2001; Wang and Cui, 2005).

First, the normality test was conducted on the first 35 samples that had been already chosen by the purposive sampling for the regression test. Those 35 samples, as mentioned before, were selected by choosing the areas with a certain percentage of vegetation cover, starting from 0% and going up to 100%. The sampling criteria fit with the index used for the regression test, namely NDVI, to resolve the relationship between the Landsat 8 OLI and LSA data for the spectral value. The sample distribution is also shown in Figure 4. The first normality test result is shown in Table 3.

Table 3. Shapiro-Wilk normality test result (first sampling)

	Kolmogorov-Smirnov			**Shapiro-Wilk**		
	Statistic	**df**	**Sig.**	**Statistic**	**Df**	**Sig.**
Percentage Vegetation	.195	35	.002	.881	35	.001

For this first sampling, the amounts from the sample with a certain percentage are not normally distributed, as seen in the Table 3. The significance value, which is less than 0.05, indicates that the samples did not meet the normal criteria. This was confirmed by a histogram of the tested sample, which shows that the percentage of vegetation (x-axis) has not been found on a normally distributed frequency (y-axis).

Because the first sample group did not pass the normality test, then another sample group was taken with same amount of samples (35) as the previous sample group. Based on the first sampling experience, the second sample selection was conducted by selecting more mixel areas than the first sampling and more mixel areas than pure pixel areas, as the purpose is to see the relationship of the spectral values in a mixel area between the Landsat 8 OLI and LSA data. The result of the normality test on the second sample test shown in Table 4 and Figure 4.

Table 4. Shapiro-Wilk normality test result (second sampling)

	Kolmogorov-Smirnov			Shapiro-Wilk		
	Statistic	df	Sig.	Statistic	df	Sig.
Shape_Area	.089	31	.200*	.967	35	.368

Table 3 shows that the Shapiro-Wilk test significance value is more than 0.05; this indicates that the sample passes the normality test requirement. This was confirmed by the histogram from that group of samples. As the normality test requirement was passed, the analysis of the sample was continued to the next stage, called a regression test. Figure 5 shows the distribution of first and second sample locations. The first and second sample locations consist of 35 samples, which were chosen using different methods, as mentioned previously.
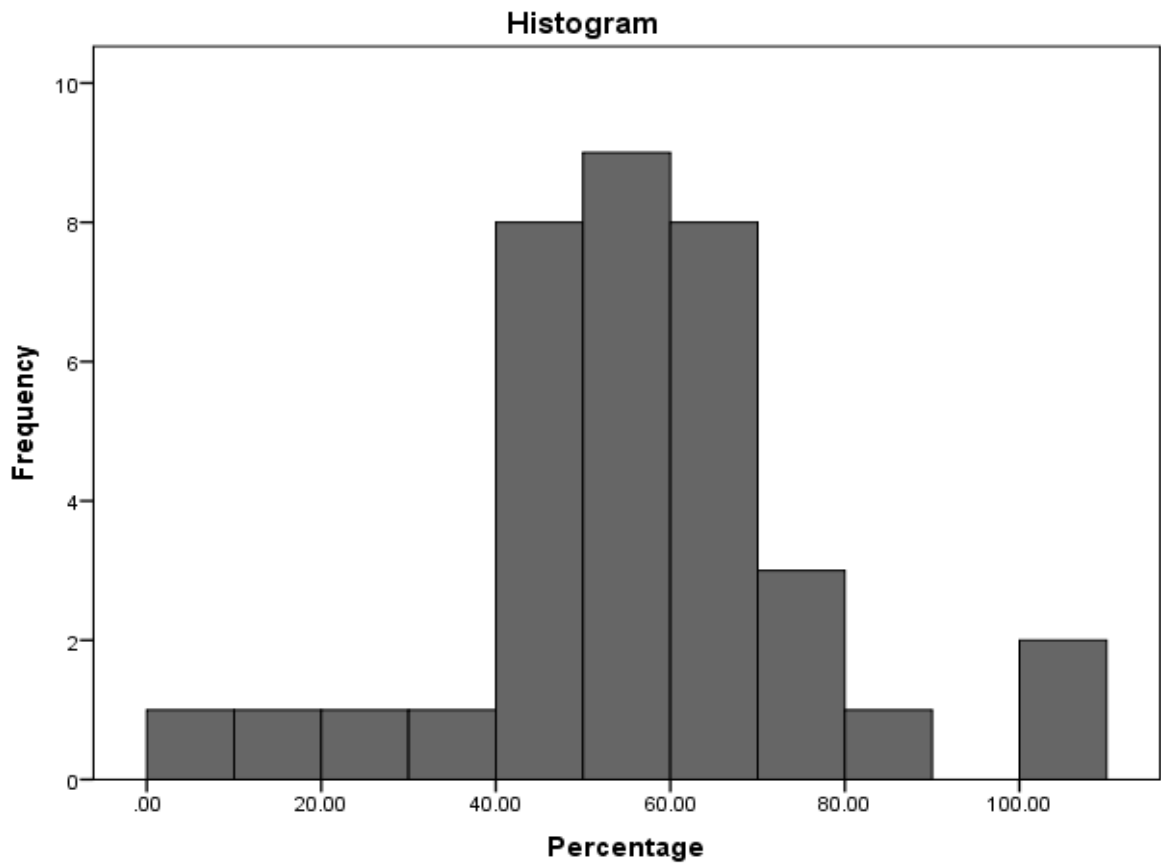
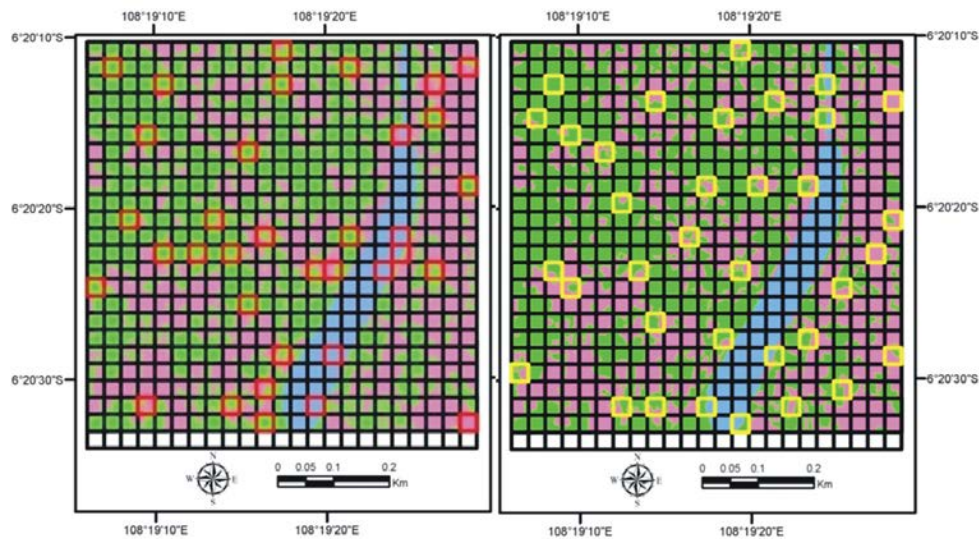*Figure 4. Histogram sample based on second sampling*

Figure 5. Distribution of the first and second sample locations

The Landsat spectral data value was transformed into a vegetation index and the result is shown in Figure 6, where the lowest value of NDVI is -0.076 and the highest value is 0.606. An NDVI value that is close to 1 shows the vegetation conditions are quite green and dense. When viewed from the Landsat composite in Figure 2, the high NDVI values, which are green, are located on the vegetation areas, while the low NDVI values (yellow through to red) are located in mixel areas and non-vegetation areas (e.g. water).
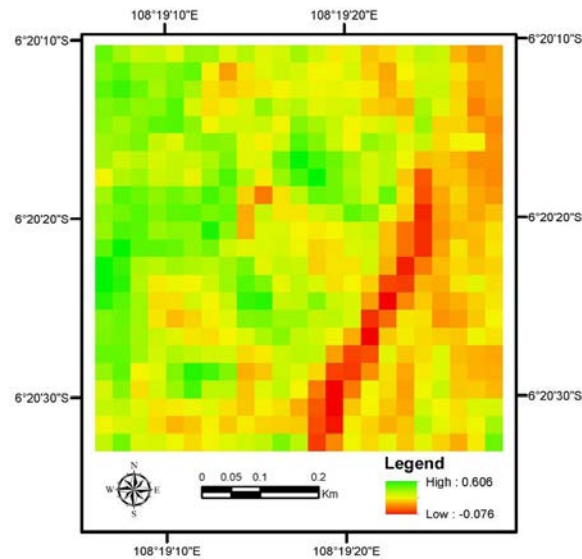
Figure 6. Transformation into the NDVI for the Landsat data

A transformation into the same index was conducted on the LSA data (Figure 7), for which the NDVI value ranges from -0.309 to 0.783. The low NDVI values, coloured red, are located on non-vegetation areas/ built-up areas. Furthermore, the high NDVI values, coloured green, are located in the vegetation land-cover areas. Table 5 shows the NDVI values for the Landsat 8 OLI and LSA using the same 30 x 30m pixel size, and the NDVI values for the LSA data are from the average of the 30 x 30m fishnet grid of the corresponding Landsat 8 OLI pixel.
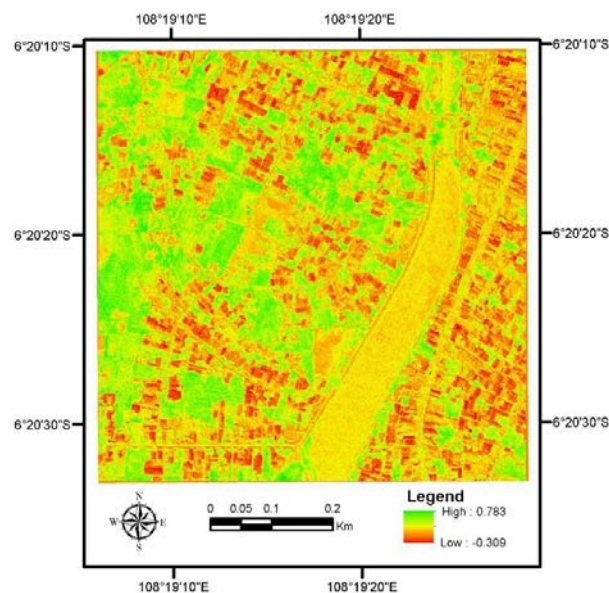

Figure 7. Transformation into the NDVI for the LSA data

There are variance of NDVI values between Landsat 8 OLI and LSA (Table 5). The LSA NDVI values, which have a higher spatial resolution, have a lower NDVI value than the Landsat 8 OLI NDVI, and there is a considerable difference between the values, except in some areas that have a grey or green highlight in Table 5. In the grey-highlighted areas, the differences in the NDVI values are not too large, while in the green-highlighted areas the NDVI value for Landsat 8 OLI is lower than the NDVI for the LSA data. The

higher spatial resolution of the LSA data means it is able to display objects with more detail and precision. As the transformation to NDVI of this data was based on the average value of all pixels in the LSA data fishnet with a size of 30 x 30 m to match the Landsat pixel in the same position, this could lead to differences between the NDVI values for the LSA and Landsat 8 OLI data, which could be caused by the detection of other objects in the LSA data on the mixel areas. In the grey- and green-highlighted areas, which consist of mixel that has a part that is a body of water, the value differences are not too large and the Landsat 8 OLI data even has a lower value than the LSA data in the green-highlighted area.

Table 5. NDVI values for the Landsat 8 OLI and LSA data

NO.	NDVI_L8	NDVI_LSA	NO.	NDVI_L8	NDVI_LSA
1	0.167	0.018	21	0.257	0.099
2	0.334	0.137	22	0.136	0.170
3	0.404	0.198	23	0.416	0.203
4	0.481	0.234	24	0.233	0.085
5	0.379	0.234	25	0.147	0.145
6	0.356	0.135	26	0.192	0.047
7	0.250	0.025	27	0.259	0.165
8	0.351	0.113	28	0.222	0.079
9	0.465	0.253	29	0.348	0.180
10	0.279	0.105	30	0.423	0.245
11	0.418	0.195	31	0.170	0.0340
12	0.334	0.110	32	0.287	0.098
13	0.328	0.136	33	0.225	0.054
14	0.271	0.077	34	0.256	0.101
15	0.343	0.144	35	0.190	0.061
16	0.373	0.156			
17	0.230	0.184			
18	0.404	0.201			
19	0.364	0.164			
20	0.276	0.084			

This phenomenon happened because of the wavelength comparison between the Landsat 8 OLI and LSA data. The wavelength of the LSA data for the green, red and NIR bands is approximately equal to TM2, TM3 and TM4 (Tetracam, 2011) as seen in Table 1. From this table, it can be observed that the NIR band for the Landsat 8 OLI data is narrower than for the LSA data, which can help with water detection (Ke *et al.*, 2015) and caused the anomalies with the grey and green highlights, where the green highlight shows that the NDVI of Landsat 8 OLI data is lower than for the LSA data, and the grey highlight shows that difference in values are not significant. After performing the normality test, the next stage was the regression test. The result of the regression test between the NDVI values for the LSA and Landsat 8 OLI data is shown in Figure 8.

The x-axis is the Landsat 8 OLI NDVI and the y-axis is the LSA NDVI. With a significance value of less than 0.05, which means there is an error rate of less than 5%, the regression equation is y = 0.520x – 0.023 with a coefficient of determination or R^2 that is 0.552, which means that the independent variables are able to explain variances of 55.2%. From the graphic in Figure 9, there are some outliers from the sample distribution and those outliers are four samples in the grey-highlighted area in Table 5.
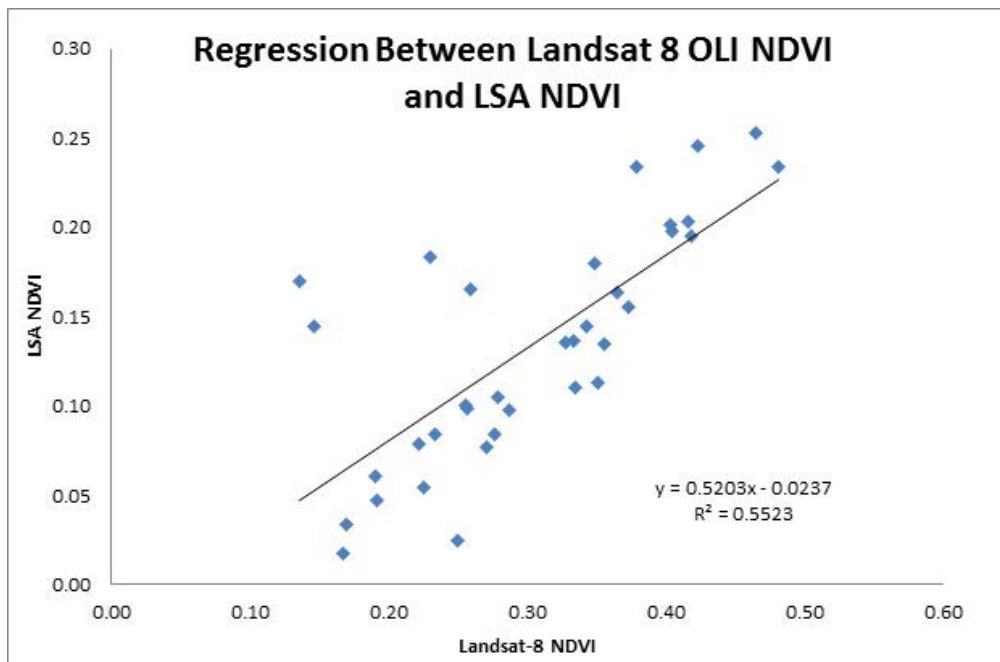
Figure 8. Regression analysis between the NDVI values for the Landsat 8 OLI data and the NDVI values for the LSA data (35 samples)
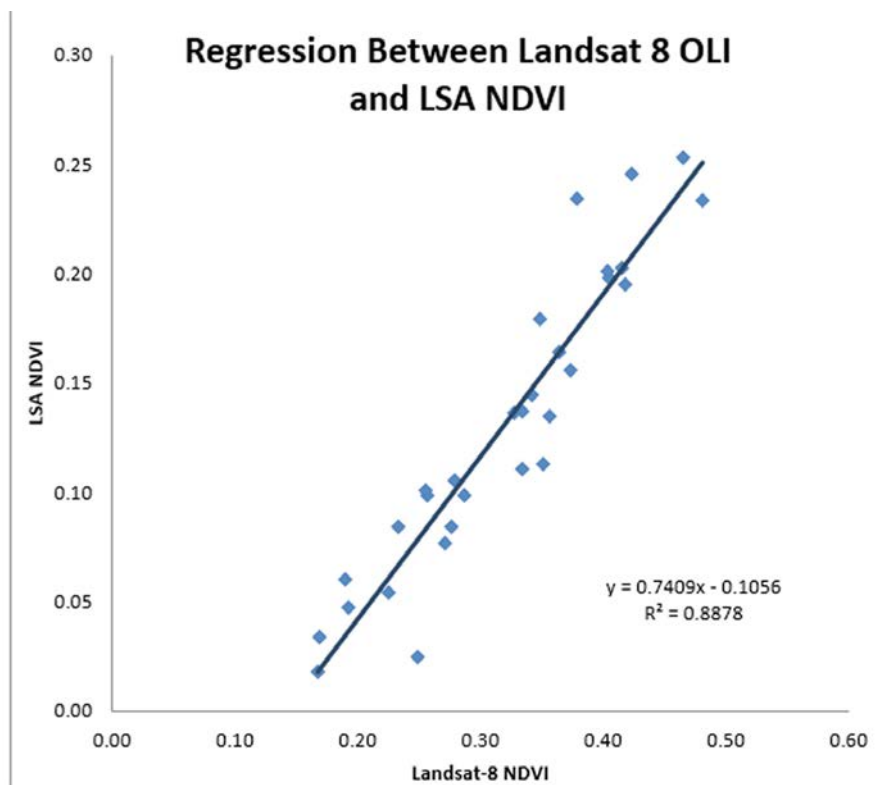

Figure 9. Regression analysis between the NDVI values for the LSA data and the NDVI values for the Landsat 8 OLI data (31 samples)

4.   Conclusion

This study examined how the 30x 30m pixel size of Landsat 8 OLI compares with the LSA data that has a spatial resolution of up to 58cm. Based on the research, it is shown that the mixel area on Landsat 8 OLI data is a mixture of several objects as seen from the LSA multispectral data. The combination created from each Landsat 8 OLI mixel includes vegetation and built-up areas, body of water and vegetation area, body of water and built-up areas, and body of water, built-up areas and vegetation. Spectrally, the

regression equation obtained by the regression analysis between the NDVI of the Landsat 8 OLI data and the NDVI of the LSA data, after the elimination of four samples containing a part that is water that were distributed in a non-linear manner (*outliers*), is y = 0.732x – 0.102 with a value of R^2= 0.887 with a significance of less than 0.05. Through these results, we can conclude that the NDVI values on both sets of data are related to one another only for dry land cover, which does not include an area that is part of a body of water.

5. Acknowledgement

6. References

Arifin, S., Annas, A., Sari, N. M., Kushardono, D. (2015) Identifikasi dan Interpretasi Visual Citra Kamera Digital Multispektral untuk Objek Wilayah Pesisir. *Prosiding Seminar Nasional Penginderaan Jauh 2015,* Bogor, Indonesia

Danoedoro, P. (2009) Penginderaan Jauh untuk Inventarisasi Mangrove; Potensi, Keterbatasan dan Kebutuhan Data. *Prosiding Workshop "Sinergi Survei dan Pemetaan Nasional dalam Mendukung Pengelolaan Mangrove Berkelanjutan",* BAKOSURTANAL Bogor 30 Juli 2009

Deichmann, U., Balk, D., & Yetman, G. (2001). Transforming population data for interdisciplinary usages: from census to grid. *Washington (DC): Center for International Earth Science Information Network*, Pp 200(1)

Fisher, P. (1997) The Pixel: A Snare and A Delusion. *International Journal of Remote Sensing,* February 1997 doi: 10.1080/014311697219015

Foody, G. M., Mathur, A. (2006) The Use of Small Training Sets Containing Mixed Pixels for Accurate Hard Image Classification: Training on Mixed Spectral Responsesfor Classification by A SVM. *Remote Sensing of Environment* 103 (2006) 179–189

Haque, M. I., Basak, R. (2017) Land Cover Change Detection Using GIS and Remote Sensing Techniques: A Spatio-temporal Study on Tanguar Haor, Sunamganj, Bangladesh. *The Egyptian Journal of Remote Sensing and Space Sciences* (2017), http://dx.doi.org/10.1016/j.ejrs.2016.12.003

Hoyano, A., Komatsu, Y. (1988) Influence of Mixels on Land Cover Classification in Residential Areas Using Airborne MSS Data. *ISPRS Archives – Volume XXVII Part B7, 1988*

Iryadi, R., Sadewo, M. N. (2015) Influence the Existence of the Bali Botanical Garden for Land Cover Change in Bedugul Basin Using Landsat Time Series. *Procedia Environmental Sciences* 24, pp. 158 – 164

Ke, Y., Im, J., Lee, J., Gong, H., Ryu, Y. (2015) Characteristics of Landsat 8 OLI-derived NDVI by Comparison with Multiple Satellite Sensors and In-situ Observations. *Remote Sensing of Environment* 164, pp. 298–313

Kurniawan, F. Adrianto, L., Bengen, D. G., Prasetyo, L. B. (2016) Patterns of Landscape Change on Small Islands: A Case of Gili Matra Islands, Marine Tourism Park, Indonesia. *Procedia Social and Behavioral Sciences* 227, pp. 553 – 559

Kushardono, D., Annas, A., Maryanto, A., Utama, A. A., Winanto (2014) Pemanfaatan Data LSA (LAPAN Dony Surveillance Aircraft) Untuk Mendukung Pemetaan Skala Rinci. Prosiding Pertemuan Ilmiah Tahunan XX MAPIN 2014, Bogor

Lv, Zhi-qiang, Qi-gang Z. (2011) Utility of Landsat Image in the Study of Land Cover and Land Surface Temperature Change. *Procedia Environmental Sciences* , pp. 1287 – 1292

Marshall, A. D., Martin, R.R. (1992) Computer Vision, Models, and Inspection. *World Scientific Series in Robotics and Automated Systems Vol. 4*

Mikovits, C., Rauch, W., Kleidorfer, M. (2014) Dynamics in Urban Development, Population Growth and Their Influences on Urban Water Infrastructure. *Procedia Engineering* 70, pp. 1147 – 1156

Mokarram, M., Boloorani, A. D., Hojati, M. (2016) Relationship between Land Cover and Vegetation Indices. Case Study: Eghlid Plain, Fars Province, Iran. *European Journal of Geography* 7(2), pp. 48 - 60

Monkkonen, P. (2013) Urban Land-use Regulations and Housing Markets in Developing Countries: Evidence from Indonesia on the Importance of Enforcement. *Land Use Policy* 34, pp.255–264

Mueller, N., Lewis, A., Roberts, D., Ring, S., Melrose, R., Sixsmith, J., Lymburner, L., McIntyre, A., Tan, P., Curnow, S., Ip, A. (2016) Water Observations from Space: Mapping Surface Water from 25 Years of Landsat Imagery across Australia. *Remote Sensing of Environment* 174, pp. 341–352

Narulita, S., Zain, A. F. M., Prasetyo, L. B. (2016) Geographic Information System (GIS) Application on Urban Forest Development in Bandung City. *Procedia Environmental Sciences* 33, pp. 279-289

Nasihin, I., Prasetyo, L. B., Kartono, A. P., Kosmaryandi, N. (2016) Land Cover Change in Kuningan District during 1994 – 2015. *Procedia Environmental Sciences* 33, pp. 428 – 435

Parsa, I. M., Yudhatama, D., Harini, S. (2014) Validasi Model Pemetaan Lahan Sawah Menggunakan Teknik Segmentasi dan Klasifikasi Citra Landsat Ortho (Studi Kasus Lampung). *Pemanfaatan Citra Penginderaan Jauh untuk Sumber Daya Wilayah Darat* ISBN No : 978-602-14437-6-7

Pour, A. B., Hashim, M. (2015) Hydrothermal Alteration Mapping from Landsat-8 Data, Sar Cheshmeh Copper Mining District, South-Eastern Islamic Republic of Iran. *Journal of Taibah University for Science 9*, pp. 155–166

Rahayu, Candra, D. S. (2014) Koreksi Radiometrik Citra Landsat-8 Kanal Multispektral Menggunakan Top of Atmosphere (ToA) untuk Mendukung Klasifikasi Penutup Lahan. *Prosiding Seminar Nasional Penginderaan Jauh 2014,* Bogor

Rawlings, J. O., Pantula, S. G., Dickey, D. A. (2001) Applied Regression Analysis: A Research Tool. *Springer Science & Business Media*

Sari, N. M., Kushardono, D. (2015) Object Segmentation on UAV Photo Data to Support the Provision of Rural Area Spatial Information. *Forum Geografi* Vol. 29 (1) July 2015 49-58

Sari, N. M., Kushardono, D. (2016) Quality Analysis of Single Tree Object with OBIA and Vegetation Index from LAPAN Surveillance Aircraft Multispectral Data in Urban Area. *Journal of Geomatics and Planning* doi: 10.14710/ geoplanning.3.2.93-106

Shapiro, S.S., Wilk, M. B. (1965) An Analysis of Variance Test for Normality (Complete Samples). *Biometrika* 52 (3): 591-611 http://www.jstor.org/stable/2333709

Sholihah, R.I., H.T., Bambang, S., Diar, S. I., La Ode, K., Selamet, Manijo, R.P., Dyah. (2016) Identification of Agricultural Drought Extent Based on Vegetation Health Indices of Landsat Data: Case of Subang and Karawang, Indonesia. *Procedia Environmental Sciences* 33 (2016) 14 – 20

Smith, A. R., Colombi, J. M., Wirthlin, J. R. (2013) Rapid Development: A Content Analysis Comparison of Literature and Purposive Sampling of Rapid Reaction Projects. *Procedia Computer Science* 16, pp. 475 – 482

Sun, X., Du, H., Han, N., Zhou, G., Lu, D., Ge, H., Xu, X., Liu, L. (2014) Synergistic Use of Landsat TM and SPOT 5 imagery for Object-Based Forest Classification. *Journal of Applied Remote Sensing* Vol. 8 2014 083550-1 - 083550-15

Tarantino, C., Adamo, M., Lucas, R., Blonda, P. (2016) Detection of Changes in Semi-Natural Grasslands by Cross Correlation Analysis with WorldView-2 Images and New Landsat 8 Data. *Remote Sensing of Environment* 175, pp. 65–72

Tetracam Inc. (2011) Agricultural Camera Digital User's Guide. Tetracam Inc. California, USA

Topp, L., Barker, B., Degenhardt, L. (2004) The External Validity of Results Derived from Ecstasy Users Recruited Using Purposive Sampling Strategies. *Drug and Alcohol Dependence* 73, pp. 33–40

Trimble Documentation (2014) Ecognition Developer Reference Book 9.0. Trimble Documentation München, Germany

USGS (2016) Landsat 8 Data Users Handbook. US Geological Survey Dept. of Interior South Dakota, USA

Vorontsova, A. V., Vorontsova, V. L., Salimgareev, D. V. (2016) The Development of Urban Areas and Spaces with the Mixed Functional Use. *Procedia Engineering* 150, pp. 1996-2000

Wang, J.X., W., Jun, Z., Fuxia. (2011) Investigate Research of Soil Erosion Base on Ikonos and Landsat Images in Jinning. *Procedia Engineering* 15, pp. 1345 – 1349

Wang, X., Cui, P. (2005) Support Soil Conservation Practices by Identifying Critical Erosion Areas within an American Watershed Using the GIS-AGNPS Model. *Journal of Spatial Hydrology* Vol. 5 No. 2 31-44

Widodo, B., Lupyanto, R., Sulistiono, B., Harjito, D. A., Hamidin, J.,Hapsari, E., M., Yasin, C., Ellinda. (2015) Analysis of Environmental Carrying Capacity for the Development of Sustainable Settlement in Yogyakarta Urban Area. *Procedia Environmental Sciences* 28 (2015) 519-527

Xing, Y., Liang, H., Xu, D. (2013) Sustainable Development Evaluation of Urban Traffic System. *Procedia Social and Behavioral Sciences* 96, pp. 496 – 504

Zald, H.S.J., Michael A.W., Joanne C.W., Thomas H., Txomin H., Geordie W.H., Nicholas C.C. (2016) Integrating Landsat pixel composites and change metrics with lidar plots to predictively map forest structure and above ground biomass in Saskatchewan, Canada. *Remote Sensing of Environment* 176, pp. 188–201